Nanotechnology

DOI: 10.1002/anie.200906927

Gold Nanorods in Photodynamic Therapy, as Hyperthermia Agents, and in Near-Infrared Optical Imaging**

Wen-Shuo Kuo, Chich-Neng Chang, Yi-Ting Chang, Meng-Heng Yang, Yi-Hsin Chien, Shean-Jen Chen, and Chen-Sheng Yeh**

Decreasing the size of a material to the nanometer scale makes it sensitive to a further decrease in size or a change in shape. Among the nanomaterials that are currently being developed, gold nanoparticles are extensively exploited in organisms because of their good stability and biocompatibility. However, in biomedical applications that require a considerably deeper penetration of near-infrared (NIR) light, in which both blood and soft tissues are highly penetrable, a different type of gold nanostructure is required. Surface plasmon resonance (SPR) is a phenomenon in which free electrons in the nanostructures collectively oscillate and scatter or absorb the incident electromagnetic wave.[1] Previous studies have demonstrated various methods of shifting the SPR of gold nanomaterials to the NIR region and shown their potential in biological applications. In the NIR region, tissue transmission is optimal owing to low scattering and energy absorption, thus providing maximum irradiation penetration through tissue and minimizing the autofluorescence of the non-target tissue.[2] There are many applications for NIR-absorbing gold nanostructures in biology, and in particular gold nanorods. For example, gold nanorods can be applied in plasmon resonance light scattering,[3] Rayleigh elastic scattering,[4] surface-enhanced Raman inelastic scattering,[5] optical coherent tomography scattering,[6] two-photon luminescent non-linear imaging,[7] and photothermal therapy.[8]

Gold nanorods have also received significant attention for their emerging potential in photothermal therapy. However, little attention has been paid to the use of nanorods combined with photosensitizers in photodynamic therapy (PDT), which is the destruction of cancer cells by the highly reactive singlet oxygen of the reactive oxygen species (ROS) produced by a photosensitizing compound and light of an appropriate wavelength.[9] Gold nanorods couple a hydrophilic and anionic photosensitizer, indocyanine green (ICG)[10] (Supporting Information, Figure S1), with light from an NIR laser emitting in the NIR region on the surface of the nanorods to produce PDT. Furthermore, the excitation and emission maxima of ICG are similar to NIR wavelengths, thus enabling ICG-conjugated gold nanorods to be utilized as an effective contrast agent in biomedical imaging.[11]

Practical applications in the early detection and destruction of cancer cells using nanomaterials have emerged in recent years, and the development of multifunctional nanomaterials is currently being pursued. Herein, we propose a medical diagnosis method that uses a lethal photochemical destruction reaction and shows that multifunctional ICG-conjugated gold nanorods can simultaneously serve as photodynamic and photothermal therapeutic agents to destroy cancer cells. Furthermore, combined PDT and hyperthermia can more efficiently extinguish cancer cells than PDT or hyperthermia treatment alone, and the system can also serve as an effective bioimaging probe in the NIR region.

Gold nanorods with a cetyltrimethylammonium bromide (CTAB) surfactant coating were synthesized using the seedless growth method.[12] To conjugate ICG on the surface, CTAB was coated on the nanorods with poly(styrene-*alt*-maleic acid) (PSMA) and ICG in sequence by an electrostatic interaction. A TEM image (Figure 1) depicts gold nanorods with an aspect ratio of approximately 3.8 (length: 35 nm, width: 9.3 nm). Owing to CTAB, the surface charge of the nanorods revealed a zeta potential of approximately 39.2 mV. PSMA polymer was then first hydrolyzed by NaOH to expose the carboxyl group and then adsorbed on the nanorods by electrostatic interactions (Supporting Information, Figure S2). Figure 1 b shows Au-PSMA nanorods with negatively charged PSMA; the Au-PSMA nanorods have a surface charge of approximately −10.7 mV. By the π–π stacking

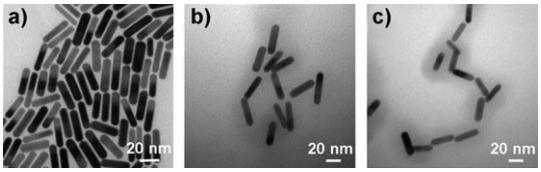

Figure 1. TEM images of a) Au nanorods, b) Au-PSMA nanorods, and c) Au-PSMA-ICG nanorods.

[*] Dr. W. S. Kuo, C. N. Chang, Y. T. Chang, Y. H. Chien, Prof. Dr. C. S. Yeh
Department of Chemistry
National Cheng Kung University, Tainan, 701 (Taiwan)
E-mail: activesitess@gmail.com
csyeh@mail.ncku.edu.tw
Dr. W. S. Kuo, Prof. Dr. S. J. Chen
Department of Engineering Science
National Cheng Kung University, Tainan, 701 (Taiwan)
M. H. Yang
Department of Life Sciences, National Chung Hsing University
Taichung, 402 (Taiwan)

[**] This work was supported by National Science Council of Taiwan.

Supporting information for this article, including experimental details, ICG and PSMA polymer structures, UV/Vis and FTIR spectra, EDX, XRD, cytotoxicity assays, Western blot, photodestruction of A549 malignant cells, singlet oxygen measurement, temperature dependence of irradiation time, fluorescence measurement, and confocal images, is available on the WWW under http://dx.doi.org/10.1002/anie.200906927.

interaction of the phenyl groups of PSMA[8d,13] with that of ICG, ICG can attach to Au-PSMA nanorods to form Au-PSMA-ICG nanorods (Figure 1c).

Gold nanorods exhibit two plasmon resonances, namely transverse plasmon (ca. 520 nm) and longitudinal plasmon (ca. 800 nm). When PSMA was coated on the nanorods, the longitudinal plasmon became a broad band and extended up to 950 nm (Supporting Information, Figure S3). The UV/Vis spectrum of ICG includes two main peaks at approximately 708 nm (the oligomeric form) and 780 nm (the monomeric form).[10b,11b] With ICG conjugation, two more bands appeared at around 720–770 nm and 830–900 nm. This change is primarily because the red-shifted absorption of ICG corresponds to dye aggregation to form dimers and trimers, and the phenyl groups of PSMA with that of ICG by π–π stacking interactions.[8d,13] After red-shifted absorption, the transverse plasmon of the gold nanorods disappeared. UV/Vis spectra show the successful conjugation results of ICG coated on the Au-PSMA nanorods. This study estimated the average ICG numbers per Au-PSMA nanorod using the Lambert–Beer law, and measured the absorbance difference of ICG at 780 nm before and after the ICG conjugation with gold nanorods. These results show that there was an average of about 28100 ICG molecules per Au-PSMA nanorod.

To further demonstrate the successful conjugation of ICG, the Au-PSMA-ICG nanorods were characterized by FTIR spectroscopy (Supporting Information, Figure S4). The characteristic IR bands show that the PSMA and ICG have been conjugated well onto the gold nanorod in sequence. EDX and XRD measurements were also employed to investigate the properties of the nanorods (Supporting Information, Figure S5). With these characterizations, the results show that PSMA and ICG were well-coated on the surface of the nanorods.

The cytotoxicity of the Au-PSMA-ICG nanorods was then examined. Cell viability experiments were conducted by incubating a human lung carcinoma malignant cell line (A549) with Au-PSMA-ICG nanorods in the dark for 24 h (all the other PDT experiments involving ICG were also carried out in the dark).[8b,14] Cell viability was nearly 100%, which is evidence of good biocompatibility (Supporting Information, Figure S6). We chose an appropriate number of gold nanorods (5×10^{11}) in experiments throughout this study.

Au-PSMA-ICG nanorods exhibit absorption in the NIR region (Supporting Information, Figure S3). As such, these biocompatible Au-PSMA-ICG nanorods might act as photothermal absorbers and photodynamic agents for destroying cancer cells with an NIR laser. The A549 cell line, which overexpresses the epidermal growth factor receptor (EGFR) on the cell surface, was used to study the hyperthermia and PDT effect of Au-PSMA-ICG nanorods. The western blot data indeed show that the amount of EGFR on the A549 surface was more than that on the human keratinocyte nonmalignant cell line (HaCaT), which lacked high expression of EGFR on the cell surface (Supporting Information, Figure S7). For specifically targeted NIR photochemical destruction, anti-EGFR antibodies (Ab_{EGFR}) were conjugated with ICG, Au-PSMA nanorods, and Au-PSMA-ICG nanorods. The anti-EGFR antibody (1 mg mL^{-1}) was mixed with all the materials by a volume ratio $V_{antibody}/V_{material}=1$. An electrostatic interaction can occur between the negatively charged ICG, Au-PSMA nanorods, and Au-PSMA-ICG nanorods and the positively charged segment of the anti-EGFR antibodies.[8c,d,f] The photodestruction of A549 cells treated with Au-PSMA-ICG nanorods was performed using a continuous-wave diode laser with a wavelength of 808 nm (output power: 22.5 W cm^{-2}, 1 mm^2 laser beam spot area). The cells were stained with calcium acetoxymethyl ester (calcein AM) indicator and incubated for another 2 h in the dark after irradiation to allow ICG to produce significant amounts of ROS and proceeding PDT.[15] Figure 2 shows the

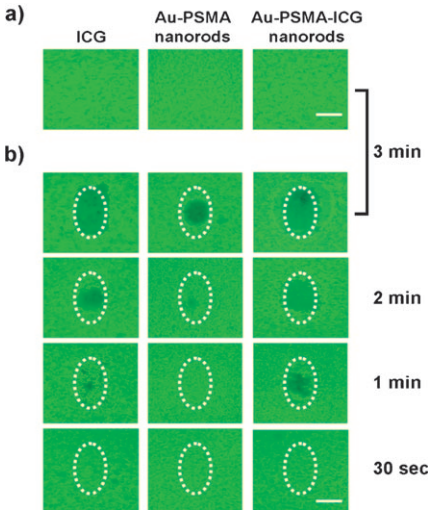

Figure 2. Photodestruction of A549 malignant cells shown by fluorescence. ICG, Au-PSMA nanorods, and Au-PSMA-ICG nanorods a) without and b) with conjugated Ab_{EGFR}-treated A549 cells, and irradiated by an NIR laser (808 nm) at 22.5 W cm^{-2} power density. Au nanorods were delivered in doses of 5×10^{11} Au nanorods. The quantities of free ICG and ICG conjugated onto Au nanorods were fixed at 2.334×10^{-4} M. The dotted circles indicate the laser beam area. The cells were stained with calcein AM and incubated for 2 h in the dark after irradiation; live cells exhibited green fluorescence. Scale bar: 1 mm.

results of exposing A549 cells to the 808 nm NIR laser for 30 seconds to 3 minutes. The A549 cells treated with ICG, Au-PSMA nanorods, and Au-PSMA-ICG nanorods without conjugation of anti-EGFR antibodies showed no loss of viability (Figure 2a). In contrast, a significant loss of viability, marked by a lack of green fluorescence, occurs after exposure of ICG-Ab_{EGFR} and Au-PSMA-ICG nanorods-Ab_{EGFR} to treatment for 1 minute, whereas A549 cells treated with Au-PSMA nanorods began at 2 minutes because of the PDT and hyperthermia effects (Figure 2b). The cells were incubated for another 2 h in the dark after irradiation and then again compared with those observed immediately after irradiation (Supporting Information, Figure S8). Owing to significant amounts of ROS produced from ICG and proceeding PDT as the incubation time increased, this comparison shows that the proportion of the void region (area of loss of live cells) spread. On the other hand, different dosage of material-Ab_{EGFR}

(dose: 5×10^{11} to 1×10^{8} gold nanorods) was also conducted with the same output power for irradiation for 2 minutes (Supporting Information, Figure S9a). The Au-PSMA-ICG nanorod dosage that caused cell death started at 1×10^{9} Au nanorods. However, ICG-treated cells remained alive at the same dose. Furthermore, the concentration of antibody conjugated on Au-PSMA-ICG nanorods was explored. The anti-EGFR antibody (1 mg mL^{-1}) was mixed with Au-PSMA-ICG nanorods (dose: 5×10^{11} Au nanorods) by a volume ratio of $V_{\text{antibody}}/V_{\text{Au-PSMA-ICG nanorods}} = 1{:}1$ to 0.001:1. After the NIR laser treatment, the void region decreased with the decrease of volume ratio; moreover, images were revealed a loss of cancer cell viability beginning at a 0.001:1 volume ratio (Supporting Information, Figure S9b). As a result, the amount of antibody on gold nanorods would be related to the efficiency of photodestruction effect. These results also indicate that the Au-PSMA-ICG nanorods seemed to improve the efficacy of PDT and photothermal reactions compared with ICG and Au-PSMA nanorod treatment alone.

Because ICG generates singlet oxygen when exposed to a 808 nm NIR laser during PDT, direct detection of singlet oxygen was carried out.[8b,16] After 30 to 120 seconds of laser exposure, the ICG alone and Au-PSMA-ICG nanorods exhibited fluorescence (Supporting Information, Figure S10). The singlet oxygen quantum yield ($\Phi_{\triangle}$) of ICG and Au-PSMA-ICG nanorods was also obtained by comparison with a reference (toluidine blue O, TBO), which was about 0.112 and 0.160, respectively.[17] To summarize these results, the Au-PSMA-ICG nanorods indeed generated more singlet oxygen than ICG alone, suggesting that Au-PSMA-ICG nanorods exhibit greater PDT efficiency. The increase in singlet oxygen caused by Au-PSMA-ICG nanorods may be due to enhanced intersystem crossing, increased triplet yield of the photosensitizers, or the metal substrates, resulting in photostability for the photosensitizers.[8b,16a]

We also examined the temperature dependence of irradiation time. The NIR irradiation-induced temperature produced by a 808 nm NIR laser changed for Au-PSMA nanorods and Au-PSMA-ICG nanorods as a function of exposure time (Supporting Information, Figure S11). The Au-PSMA-ICG nanorods increased in temperature rapidly to around 46 °C after 1 minute of irradiation time. Note that tumor cells can be destroyed over a temperature range of 42–47 °C.[8d,18] The temperature curve of Au-PSMA nanorods had a similar trend, but showed a lower degree of temperature elevation. In contrast, water had no apparent increase after laser irradiation. Therefore, Au-PSMA-ICG nanorods are able to produce more singlet oxygen for PDT than ICG, and can simultaneously act as effective photothermal mediators.

To better understand the efficiency of the photodestruction shown in Figure 2, the integrated green fluorescence light intensity was then divided by the fluorescence intensity of the control cells, producing cell viability (%);[8d] the laser beam spot is indicated by dotted circles.[19] Data were expressed as the mean ± standard deviation, and their statistical differences were assessed by Student's t test. The control cells without any treatment were irradiated at the same NIR laser power and illumination conditions. Without nanorod treatment, the A549 cells showed no damage after laser exposure (Figure 3); however, the viability of the ICG-treated and Au-PSMA-ICG nanorod-treated A549 cells fell to approximately 69.4 % and 55.4 % ($p < 0.0001$ for the viability compared with each other), respectively, after 2 minutes of laser exposure. Viability fell significantly to about 8.3 % and 2 % ($p < 0.0001$ for the viability compared with each other) after 3 minutes of laser irradiation, whereas viability of Au-PSMA nanorods only decreased to 92.6 % and 69 % for 2 minutes and 3 minutes of irradiation, respectively. Au-PSMA-ICG nanorods were better able to kill cancer cells than ICG and Au-PSMA nanorods for both 2 minute and 3 minute laser exposure times. The purely additive interaction of PDT and hyperthermia were calculated using $P_{\text{Additive}} = (f_A \times f_B)P_0$,[20] where P_{Additive} is the final population after an additive interaction, P_0 is the initial population, f_A is the cell viability after PDT treatment, and f_B is cell viability after hyperthermia treatment. The predicted additive was estimated at about 65.6 % and 5.9 % for 2 minutes and 3 minutes of irradiation, respectively. Cell viability of Au-PSMA-ICG nanorod-treated cells compared with that of predicted additive ($p = 0.0004$ and $p < 0.0001$ for 2 minutes and 3 minutes of irradiation, respectively) was statistically significant. According to these data, there was indeed an additive effect in the therapeutic efficacy of Au-PSMA-ICG nanorods. The resulting Au-PSMA-ICG nanorods simultaneously served as PDT and hyperthermia agents. Combined PDT and hyperthermia killed cancer cells more efficiently than PDT or hyperthermia treatment alone, and improved photodestruction efficiency as well.

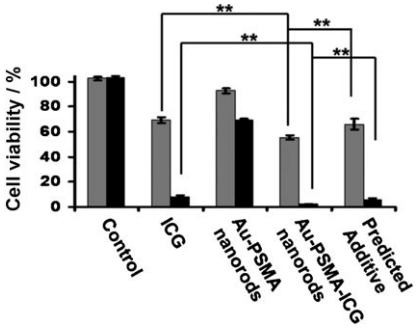

Figure 3. Cell viability estimation of ICG, Au-PSMA nanorods, and Au-PSMA-ICG nanorods with conjugated Ab_{EGFR}-antibody-treated A549 cells by exposure to an NIR laser (808 nm) at 22.5 W cm^{-2} power density. Au nanorod dose: 5×10^{11}; 2.334×10^{-4} M of free ICG and ICG conjugated onto Au nanorods. Gray bars: 2 min laser exposure; black: 3 min. Data expressed as the mean ± SD ($n = 10$). ** $p < 0.01$ by the Student's t test.

By integration of the advantages of Au-PSMA-ICG nanorods, multimodal imaging agents with hyperthermia, PDT, and optical imaging capabilities had great potential in cancer therapy, diagnosis, targeted molecular imaging, and the monitoring of the therapeutic effects simultaneously. Owing to the excitation and emission maxima of ICG in the NIR region (808 nm excitation, 820 nm emmision), which was able to avoid relatively transparent media, such as blood and tissues, and minimize complications from the intrinsic back-

ground interference, it is suitable for being utilized as a contrast agent for biomedical imaging.[10c,11] Figure 4 shows the images of A549 cancer cells treated with Au-PSMA-ICG nanorod-Ab_{EGFR} and ICG-Ab_{EGFR}. A549 cells treated with

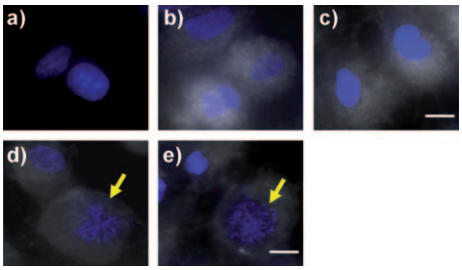

Figure 4. Confocal laser scanning images of A549 cells a) without ICG treatment or laser exposure, b) with ICG but without laser exposure, c) with Au-PSMA-ICG nanorods but without laser exposure, d) with ICG treatment and laser exposure, and e) with Au-PSMA-ICG nanorods and with laser exposure. Au nanorod dose: 5×10^{11}; 2.334×10^{-4} M of free ICG and ICG conjugated onto Au nanorods. The nuclei were stained with DAPI (blue). Scale bar: 20 μm.

ICG-Ab_{EGFR} and Au-PSMA-ICG nanorod-Ab_{EGFR} without NIR laser exposure showed ICG and Au-PSMA-ICG nanorods were taken into cells and showed significant NIR fluorescence in the cytoplasm (Figure 4b,c). Although gold is known to quench other fluorescence, metal-enhanced fluorescence (MEF) is a phenomenon in which the quantum yield and photostability of weakly fluorescent species are dramatically increased owing to the proximity of free electron-rich metals, such as noble metals. In this condition, excited state fluorophores behave as oscillating dipoles that interact with free electrons in noble metals. These interactions can increase the radiative decay rate of the fluorophores, resulting in increasing quantum yields, which in turn enhances the fluorescence of the noble metals. The increasing intensities of ICG are also associated with decreased lifetimes and increased photostability.[21] We monitored the emission fluorescence intensity of Au-PSMA-ICG nanorods at 815 nm wavelength and noted it increased about 26% as compared to that of ICG (Supporting Information, Figure S12). As a result, the surface noble metals display high chemical stability and are promising for MEF.[22] Therefore, Au-PSMA-ICG nanorods in this study may become a powerful tool in medical diagnostics and imaging applications. Figure 4d,e show that A549 cells started to undergo PDT and were damaged by NIR laser irradiation (22.5 $W\,cm^{-2}$ power density for 2 minutes). The cancer cells depicted the morphology of nuclear cleavage of DNA (indicated by yellow arrows in Figure 4d,e), and apoptotic body going to formation. ICG and nanorods exhibit weak NIR fluorescence images after NIR laser exposure. This effect could be because the cells were then washed several times with PBS buffer, according to routine procedures, to remove ICG and nanorods or efflux from the cytoplasm. These results also imply that the irradiated cells were indeed damaged because the permeability of the cell membrane increased with laser irradiation. With differential interference contrast (DIC) images merged, the localization of Au-PSMA-ICG nanorods can be observed inside cells by the fluorescence from ICG; moreover, the images showed the cellular morphology after irradiation (Supporting Information, Figure S13). Furthermore, the UV/Vis spectra of ICG exposed to a NIR laser reveal that laser-treated ICG ablated the surface plasmon resonance. The absorbance of ICG did not obviously decrease, and there was no change in the color of ICG, even after 3 minutes of laser exposure (Supporting Information, Figure S14). There was no apparent irreversible degredation of ICG even using these experimental processes. These results indicate that the Au-PSMA-ICG nanorods can serve as an effective and stable bio-nanoprobe to track and monitor the localization of nanorods interior cells and provide additional imaging in cellular morphology by laser exposure. This imaging contrast agent is therefore expected to be applicable in clinical therapy and diagnosis in the future.

In summary, Au-PSMA-ICG nanorods have been successfully prepared to simultaneously serve as PDT and hyperthermia agents with improved photodestruction efficacy and to act as an effective bioimaging probe in the NIR region.

Received: December 8, 2009
Revised: January 11, 2010
Published online: March 16, 2010

Keywords: gold · hyperthermia · imaging agents · nanostructures · photodynamic therapy

[1] U. Kreibig, M. Vollmer, *Optical Properties of Metal Clusters*, Springer, New York, **1995**.
[2] a) I. H. El-Sayed, X. Huang, M. A. El-Sayed, *Nano Lett.* **2005**, *5*, 829–834; b) C. Radloff, R. A. Vaia, J. Brunton, G. T. Bouwer, V. K. Ward, *Nano Lett.* **2005**, *5*, 1187–1189; c) R. Weissleder, *Nat. Biotechnol.* **2001**, *19*, 316–317.
[3] J. Nappa, G. Revillod, J. P. Abid, I. Russier-Antoine, C. Jonin, E. Benichou, H. H. Giraultb, P. F. Brevet, *Faraday Discuss.* **2004**, *269*, 935–939.
[4] A. K. Singh, D. Senapati, S. Wang, J. Griffin, A. Neely, P. Candice, K. M. Naylor, B. Varisli, J. R. Kalluri, P. C. Ray, *ACS Nano* **2009**, *3*, 1906–1912.
[5] Q. Liao, C. Mu, D. S. Xu, X. C. Ai, J. N. Yao, J. P. Zhang, *Langmuir* **2009**, *25*, 4708–4714.
[6] L. Oldenburg, M. N. Hansen, D. A. Zweifel, A. Wei, S. A. Boppart, *Opt. Express* **2006**, *14*, 6724–6738.
[7] N. J. Durr, T. Larson, D. K. Smith, B. A. Korgel, K. Sokolov, A. Ben-Yakar, *Nano Lett.* **2007**, *7*, 941–945.
[8] a) W. S. Kuo, C. M. Wu, Z. S. Yang, S. Y. Chen, C. Y. Chen, C. C. Huang, W. N. Li, C. K. Sun, C. S. Yeh, *Chem. Commun.* **2008**, 4430–4432; b) W. S. Kuo, C. N. Chang, Y. T. Chang, C. S. Yeh, *Chem. Commun.* **2009**, 4853–4855; c) K. W. Hu, C. C. Huang, J. R. Hwu, W. C. Su, D. B. Shieh, C. S. Yeh, *Chem. Eur. J.* **2008**, *14*, 2956–2964; d) C. C. Huang, C. H. Su, W. M. Li, T. Y. Liu, J. H. Chen, C. S. Yeh, *Adv. Funct. Mater.* **2009**, *19*, 249–258; e) L. R. Hirsch, R. J. Stafford, J. A. Bankson, S. R. Sershen, B. Rivera, R. E. Price, J. D. Hazle, N. J. Halas, J. L. West, *Proc. Natl. Acad. Sci. USA* **2003**, *100*, 13549–13554; f) X. Huang, I. H. El-Sayed, W. Qian, M. A. El-Sayed, *J. Am. Chem. Soc.* **2006**, *128*, 2115–2120; g) J. Kim, Y. Piao, T. Hyeon, *Chem. Soc. Rev.* **2009**, *38*, 372–390.
[9] a) E. J. Dennis, G. J. Dolmans, D. Fukumura, R. K. Jain, *Nat. Rev. Cancer* **2003**, *3*, 380–387; b) F. Gad, T. Zahra, K. P. Francis, T. Hasan, M. R. Hamblin, *Photochem. Photobiol. Sci.* **2004**, *3*, 451–458; c) M. L. Embleton, S. P. Nair, B. D. Cookson, M.

Wilson, *J. Antimicrob. Chemother.* **2002**, *50*, 857 – 864; d) C. S. Foote, *Photochem. Photobiol.* **1991**, *54*, 659; e) L. R. Jones, L. I. J. Grossweiner, *J. Photochem. Photobiol. B* **1994**, *26*, 249 – 256; f) M. Merchat, G. Bertolini, P. Giacomini, A. Villanueva, G. Jori, *J. Photochem. Photobiol. B* **1996**, *32*, 153 – 157; g) M. T. Jarvi, M. J. Niedre, M. S. Patterson, B. C. Wilson, *Photochem. Photobiol.* **2006**, *82*, 1198 – 1210.

[10] a) I. Fox, G. Brooker, D. Heseltine, H. Essex, E. Wood, *Am. J. Physiol.* **1956**, *187*, 599 – 606; b) K. Urbanska, B. Romanowska-Dixon, Z. Matuszak, J. Oszajca, P. Nowak-Sliwinska, G. Stochel, *Acta Biochim. Pol.* **2002**, *49*, 381 – 391; c) C. H. Lee, S. H. Cheng, Y. J. Wang, Y. C. Chen, N. T. Chen, J. Souris, C. T. Chen, C. Y. Mou, C. S. Yang, L. W. Lo, *Adv. Funct. Mater.* **2009**, *19*, 215 – 222.

[11] a) Y. T. Lim, Y. W. Noh, J. H. Han, Q. Y. Cai, K. H. Yoon, B. H. Chung, *Small* **2008**, *4*, 1640 – 1645; b) T. Desmettre, J. M. Devoisselle, S. Mordon, *Surv. Ophthalmol.* **2000**, *46*, 15 – 27.

[12] C. Liao, J. Roider, D. G. Jay, *Proc. Natl. Acad. Sci. USA* **1994**, *91*, 2659 – 2663.

[13] a) D. C. Barber, R. A. Freitag-Beeston, D. G. Whitten, *J. Phys. Chem.* **1991**, *95*, 4074 – 4086; b) G. Pagona, A. S. D. Sandanayaka, Y. Araki, J. Fan, N. Tagmatarchis, M. Yudasaka, S. Iijima, O. Ito, *J. Phys. Chem. B* **2006**, *110*, 20729 – 20732.

[14] a) V. Decraene, J. Prattern, M. Wilson, *Appl. Environ. Microb.* **2006**, *72*, 4436 – 4439; b) M. Sharma, L. Visai, F. Bragheri, I. Cristiani, P. K. Gupta, P. Speziale, *Antimicrob. Agents Chemother.* **2008**, *52*, 299 – 305; c) J. Gil-Tomás, S. Tubby, I. P. Parkin, N. Narband, L. Dekker, S. P. Nair, M. Wilson, C. Street, *J. Mater. Chem.* **2007**, *17*, 3739 – 3746.

[15] D. Gao, R. R. Agayan, H. Xu, M. A. Philbert, R. Kopelman, *Nano Lett.* **2006**, *6*, 2383 – 2386.

[16] a) Y. Zhang, K. Aslan, M. J. R. Previte, C. D. Geddes, *J. Fluoresc.* **2007**, *17*, 345 – 349; b) Y. Zhang, K. Aslan, M. J. R. Previte, C. D. Geddes, *Proc. Natl. Acad. Sci. USA* **2008**, *105*, 1798 – 1802; c) X. Ragas, A. Jimenez-Banzo, D. Sanchez-Garcia, X. Batllori, S. Nonell, *Chem. Commun.* **2009**, 2920 – 2922.

[17] a) R. Schmidt, C. Tanielian, *J. Phys. Chem. A* **2000**, *104*, 3177 – 3180; b) C. M. de Mello Donegá, S. G. Hickey, S. F. Wuister, D. Vanmeakelbergh, A. Meijerink, *J. Phys. Chem. B* **2003**, *107*, 489 – 496; c) N. A. Romanova, L. Y. Brovko, L. Moore, E. Pometun, A. P. Savitsky, N. N. Ugarova, M. W. Griffiths, *Appl. Environ. Microbiol.* **2003**, *69*, 6393 – 6398; d) J. A. Cardillo, R. Jorge, R. A. Costa, S. M. T. Nunes, D. Lavinsky, B. D. Kuppermann, A. C. Tedesco, M. E. Farah, *Br. J. Ophthalmol.* **2008**, *92*, 276 – 280; e) K. K. Chin, C. C. Trevithick-Sutton, J. McCallum, S. Jockusch, N. J. Turro, J. C. Scaiano, C. S. Foote, M. A. Garcia-Garibay, *J. Am. Chem. Soc.* **2008**, *130*, 6912 – 6913; f) J. A. Bonacin, F. M. Engelmann, D. Severino, H. E. Toma, M. S. Baptista, *J. Braz. Chem. Soc.* **2009**, *20*, 31 – 36.

[18] L. R. Hirsch, R. J. Stafford, J. A. Bankson, S. R. Sershen, B. Rivera, R. E. Price, J. D. Hazle, N. J. Halas, J. L. West, *Proc. Natl. Acad. Sci. USA* **2003**, *100*, 13549 – 13554.

[19] K. W. Hu, T. M. Liu, K. Y. Chung, K. S. Huang, C. T. Hsieh, C. K. Sun, C. S. Yeh, *J. Am. Chem. Soc.* **2009**, *131*, 14186 – 14187.

[20] a) T. S. Hauck, T. L. Jennings, T. Yatsenko, J. C. Kumaradas, W. C. W. Chan, *Adv. Mater.* **2008**, *20*, 3832 – 3838; b) G. M. Hahn, J. Braun, I. Har-Kedar, *Proc. Natl. Acad. Sci. USA* **1975**, *72*, 937 – 940.

[21] K. Aslan, S. N. Malyn, C. D. Geddes, *J. Fluoresc.* **2007**, *17*, 7 – 13.

[22] a) R. R. Chance, A. Prock, R. Silbey, *Adv. Chem. Phys.* **1978**, *37*, 1 – 65; b) J. I. Gersten, A. Nitzan, *Chem. Phys. Lett.* **1984**, *104*, 31 – 37; c) J. I. Gersten, A. Nitzan, *J. Chem. Phys.* **1981**, *75*, 1139 – 1152; d) C. D. Geddes, H. Cao, I. Gryczynski, Z. Gryzzynski, J. Fang, J. R. Lakowicz, *J. Phys. Chem. A* **2003**, *107*, 3443 – 3449.

